Biomimetic Design and Kinematic Analysis of a Rope-driven Soft Robotic Arm

1st Ruile Ma
School of Electrical and Information Engineering
Zhengzhou University
Zhengzhou, China
2521394302@qq.com

2nd Jinzhu Peng*
School of Electrical and Information Engineering
Zhengzhou University
Zhengzhou, China
jzpeng@zzu.edu.cn

3rd Pengfei Yu
School of Electrical and Information Engineering
Zhengzhou University
Zhengzhou, China
2816148757@qq.com

4th Nan Zhao
Department of Artificial Intelligence Business
Zhengzhou JD Cloud Computing Co., Ltd.
Zhengzhou, China
zhaonan8@jd.com

2024 9th International Conference on Automation, Control and Robotics Engineering (CACRE) | 979-8-3503-5030-2/24/$31.00 ©2024 IEEE | DOI: 10.1109/CACRE62362.2024.10635043

***Abstract*—Soft robotic arms have strong adaptability and their broad application prospects have been attracted increasing attention. In this paper, the structure of a kind of rope-driven soft robotic arm is designed based on the biological characteristics, and its kinematic model is established based on constant curvature analysis. The spatial posture and end position of the soft robotic arm are obtained through numerical simulations, and the results reveal the reachable workspace of the designed soft robotic arm. In addition, based on the inverse kinematics of soft robotic arm, the circular trajectory planning is analyzed and discussed. The experimental results of spatial posture and trajectory planning are consistent with the simulation results, which indicates that the designed soft robotic arm structure is reasonable and the kinematic analysis is correct.**

***Keywords*—soft robotic arm, biomimetic design, kinematic analysis, circular trajectory planning**

I. Introduction

Most of the traditional rigid robotic arms are assembled by components with certain hardness, which have low safety and poor movement flexibility when contacting with people and fragile objects. Especially in the face of unstructured complex environments, traditional robotic arms are difficult to efficiently complete tasks due to their rigid structure. The development of bionics has brought inspiration to the emergence of soft robotic arms. The difference between soft robotic arms and conventional robotic arms is that their partial structures are made of soft materials [1]. Soft robotic arms can flexibly change their shapes in complex environments and complete some tasks that traditional rigid robotic arms cannot accomplish.

According to different driving modes, soft robotic arms can be divided into gas-driven, shape memory alloy-driven, electroactive polymer-driven, rope-driven, and so on [2]. The pneumatic soft robotic arms have high adaptability, but there are also many drawbacks, sucn as low effective load capacity, large energy consumption, complex gas transmission system, slow response speed, and high production standard [3]. Although the full body weight of the robotic arms driven by electroactive polymer and shape memory alloy is light, the output force generated is small. In addition, higher power requirements and specific temperature changes are required, and the shape changes are limited [4,5]. The rope-driven soft robotic arms have high research value due to structural stability, operability and positioning accuracy, but it is difficult to wrap larger objects because of the length of rope [6].

Soft materials give the soft robotic arms excellent flexibility and security, but they also bring great difficulties to theoretical analysis, especially modeling. At present, the main modeling methods of soft robotic arms include finite element modeling, constant curvature modeling, variable curvature modeling, and data-driven modeling. The finite element modeling has good universality, but its cost is high and the process is complex [7]. The method of constant curvature modeling is simple, computationally efficient, and more suitable to model-based control [8]. Currently, it is the most widely used, but its accuracy is relatively low. Although the accuracy of the variable curvature modeling method has improved, its calculation is complicated, which is not applicable for model-based control [9]. The data-driven modeling has strong applicability, but data collection and training are difficult [10].

The main work of this article is as follows: Firstly, the structure of a kind of rope-driven soft robotic arm is designed by learning biological features, and the ingenious and novel biomimetic design enables the soft robotic arm to have multiple working modes, stronger adaptability, and higher stability. Secondly, based on the assumption of constant curvature, kinematic analysis is conducted on the soft robotic arm to achieve precise posture control. Thirdly, simulations of spatial posture and workspace are carried out, and experiments are

This work is supported in part by the National Natural Science Foundation of China (62273311, 61773351), and in part by Henan Provincial Science Foundation for Distinguished Young Scholars (242300421051), and in part by Zhengzhou JD Cloud Computing Co., Ltd.

conducted on the actual prototype. The consistency between simulation results and experimental results verifies the rationality of the structural design and the effectiveness of forward kinematics. Finally, the circular trajectory planning is analyzed and discussed based on inverse kinematics, which verifies the correctness of inverse kinematics.

II. Biomimetic Design and Manufacture

Through observation, the elephant's trunk is very flexible, it can easily roll up heavy objects, and the liquid suction experiment shown in Fig. 1 demonstrates that the elephant's trunk can absorb different objects [11]. Introducing this versatility into the design of a robotic arm can make it more adaptable and diverse in different scenarios and tasks. In addition, the lamellae on gecko's toes can enhance contact adaptation and reduce contact impacts [12]. The similar lamellae on the surface of a robotic arm can enhance the contact adaptability, and improve its stability when wrapping objects. As shown in Fig. 1, we produce an actual prototype of a biomimetic rope-driven soft robotic arm based on the designed 3D model by the idea of the elephant's trunk and the lamellae on the gecko's toes.

To achieve stable structure, strong operability, and high positioning accuracy, we design a rope-driven soft robotic arm. The arm body is a hollow structure made of silicone, and the spring skeleton set in the cavity is similar to the longitudinal muscles of the elephant's trunk, providing structural support and deformation ability to adapt to different working conditions. The air pipe passes through the inner cavity of the spring skeleton, connecting the air pump and the suction cup at the end of the arm. When it is difficult to wrap due to the rope length limitation, the suction cup functions as an elephant's nostril to adsorb objects, compensating for the shortcomings of the rope-driven method. The lamellae on the surface of the arm can improve the contact adaptability, adapt to different shapes of object surfaces, and improve stability and controllability when wrapping objects. The four fishing lines distributed evenly in the arm body, are pulled by four servos assembled on the base of the robotic arm to deflect and bend the arm body.

To sum up, the soft robotic arm can achieve two functions of wrapping and adsorbing objects, with high flexibility and adaptability. Compared with other robotic arms, the soft robotic arm can adapt to unstructured complex environments and complete diverse tasks more efficiently.

III. Kinematic Analysis

According to experimental observations, it can be concluded that the curvature of each part of the arm during bending is basically consistent, indicating that the bending shape of the robotic arm is approximately circular arc. Becasue the robotic arm only perform simple movements, we can use constant curvature modeling to analyze reasonably and simplify calculations. We propose three assumptions based on the above observation.

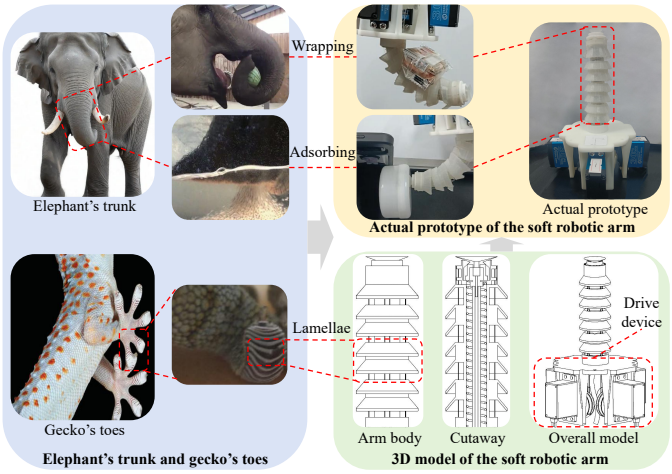

Fig. 1. Biomimetic desigh and manufacture of the soft robotic arm.

Assumption1: The bending curvature of the arm body is a constant.

Assumption2: Neglecting the influence of gravity on the bending of the arm body.

Assumption3: The shape of the arm body is simplified to a cylinder.

Define three bending parameters (ϕ θ r) based on the above assumptions [13], ϕ is the deflection angle between the plane where the arm body is located and the xoz plane, θ is the central angle, and r represents the bending radius.

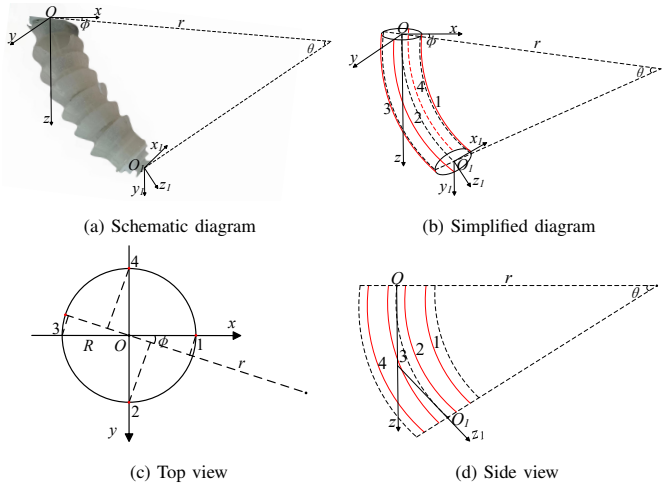

(a) Schematic diagram (b) Simplified diagram

(c) Top view (d) Side view

Fig. 2. Kinematic analysis of constant curvature.

The change of fishing line's length can be expressed as,

$$l_i = L - q_i \tag{1}$$

where L is the original length of each fishing line, q_i and l_i, $i = 1, 2, 3, 4$ are changing length and current length of each fishing line in the arm body. By analyzing, we can get,

$$\begin{cases} l = \frac{1}{4}\sum_{i=1}^{4} l_i \\ q = \frac{1}{4}\sum_{i=1}^{4} q_i \end{cases} \tag{2}$$

where q and l represent the changing length and current length of the central arc of the arm.

From Fig. 2 (c) and (d), the current length of each fishing line can be represented by bending parameters as,

$$\begin{cases} l_1 = \theta(r - R\cos\phi) \\ l_2 = \theta(r - R\sin\phi) \\ l_3 = \theta(r + R\cos\phi) \\ l_4 = \theta(r + R\sin\phi) \end{cases} \tag{3}$$

where R represents the cross section radius of the arm body. According to (1), (2), and (3), bending parameters can be expressed as,

$$\phi = \arctan\frac{q_4 - q_2}{q_3 - q_1} \tag{4}$$

$$\theta = \frac{\sqrt{(q_3 - q_1)^2 + (q_4 - q_2)^2}}{2R} \tag{5}$$

$$r = \frac{2(L - q)R}{\sqrt{(q_3 - q_1)^2 + (q_4 - q_2)^2}} \tag{6}$$

Changing length of each fishing line in the arm body can be represented as,

$$q_i = \xi_i R_d \tag{7}$$

where ξ_i and R_d represent the rotation angle and radius of servo disk, respectively. Then, by substituting (7) into (4), (5) and (6), bending parameters can be expressed as,

$$\phi = \arctan\frac{\xi_4 - \xi_2}{\xi_3 - \xi_1} \tag{8}$$

$$\theta = \frac{\sqrt{(\xi_3 - \xi_1)^2 + (\xi_4 - \xi_2)^2}}{2R} \tag{9}$$

$$r = \frac{2(L - q)R}{\sqrt{(\xi_3 - \xi_1)^2 + (\xi_4 - \xi_2)^2}} \tag{10}$$

where $q = \frac{1}{4}R_d\sum_{i=1}^{4}\xi_i$, and the forward kinematics is completed through the above steps.

The motion process of the arm body can be regarded as two steps: the soft robotic arm firstly rotates angle θ around the y-axis and then rotates angle ϕ around the z-axis [14]. The homogeneous transformation matrix from the origin of the base coordinate system to the origin of the end coordinate system can be obtained according to the two-step motion transformation as,

$$\begin{aligned} T &= \begin{bmatrix} R_z(\phi) & 0 \\ 0 & 1 \end{bmatrix}\begin{bmatrix} R_y(\theta) & p \\ 0 & 1 \end{bmatrix} \\ &= \begin{bmatrix} \cos\phi\cos\theta & -\sin\phi & \cos\phi\sin\theta & \frac{l\cos\phi(1-\cos\theta)}{\theta} \\ \sin\phi\cos\theta & \cos\phi & \sin\phi\sin\theta & \frac{l\sin\phi(1-\cos\theta)}{\theta} \\ -\sin\theta & 0 & \cos\theta & \frac{l\sin\theta}{\theta} \\ 0 & 0 & 0 & 1 \end{bmatrix} \end{aligned} \tag{11}$$

The pose matrix of the endpoint can be expressed as,

$$T_p = \begin{bmatrix} \alpha_x & \beta_x & \gamma_x & p_x \\ \alpha_y & \beta_y & \gamma_y & p_y \\ \alpha_z & \beta_z & \gamma_z & p_z \\ 0 & 0 & 0 & 1 \end{bmatrix} \tag{12}$$

where $p(p_x, p_y, p_z)$ represents the endpoint's coordinate, $(\alpha_x, \alpha_y, \alpha_z)^T$, $(\beta_x, \beta_y, \beta_z)^T$, and $(\gamma_x, \gamma_y, \gamma_z)^T$ represent the direction vector of the axis of the endpoint coordinate system in the base coordinate system, respectively.

Let $T_p = T$, we have,

$$\phi = \arctan(\frac{p_y}{p_x}) \tag{13}$$

$$\theta = 2\arctan(\frac{p_y}{p_z\sin\phi}) \tag{14}$$

$$r = \frac{p_z}{\sin\theta} \tag{15}$$

By substituting (13), (14) and (15) into (1), (3) and (7), the rotation angle of the servo disk can be obtained according to the coordinates of the endpoint or spatical posture, completing the analysis of the inverse kinematics.

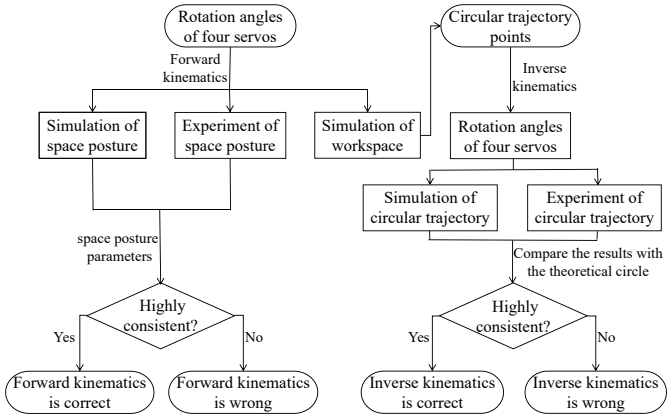

Fig. 3. Kinematic correctness verification flow chart.

As shown in Fig. 3, the subsequent content of this article will validate the correctness of the kinematic analysis mentioned above. Correct kinematic analysis is crucial for achieving precise control and highly efficient motion of the soft robotic arm.

IV. Verification of Forward Kinematics

In this part, we verify the correctness of forward kinematic analysis by comparing the simulation and experimental spatial postures. Firstly, we draw the spatial postures of the arm through simulation under different inputs. Subsequently, the Monte Carlo method is employed to compute the precise spatial position of the endpoint, and the workspace of the arm can be obtained. Finally, we conduct experiments on the actual prototype and compare the experimental results with simulation results under the same inputs.

A. Simulation of spatial posture

Because the shape of the arm body is simplified to a cylinder, the shape of the central axis and the outline of the column core are shown only during the simulation. The spatial postures can be obtained when the inputs of four servos are given. Some spatial posture simulation results are shown in Fig. 4, which indicate excellent bending performance. In addition, the different spatial postures can make the robotic arm adapt to various environments.

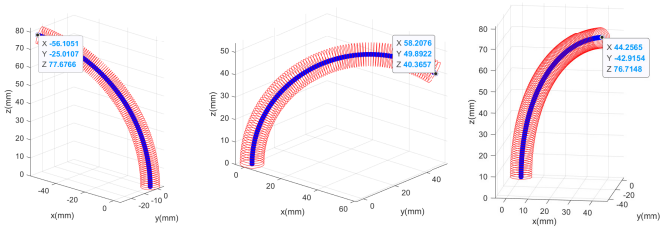

(a) (b) (c)

Fig. 4. Some simulation results of spatial posture.

B. Simulation of workspace

A commonly employed method for simulating and analyzing the workspace of robotic arms is the Monte Carlo method. Based on the principle of random sampling, it can randomly select points in the joint activity space of the robotic arm, and calculate the coordinate values corresponding to the random points through simulation. When the sampled data is sufficient, the workspace of the robotic arm can be obtained. It is specified that the variation range of the four servos is [-90°, 90°], and 125000 points are randomly generated within this range. The simulation result of the workspace is shown in Fig. 5.

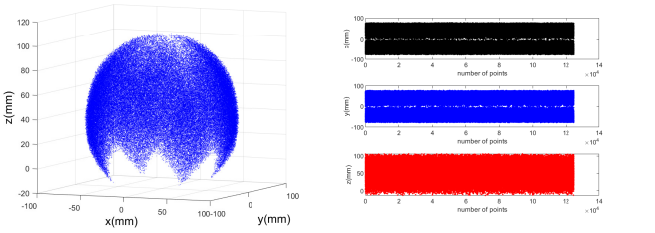

(a) Workspace simulation result (b) Range of coordinates at the endpoints

Fig. 5. Workspace simulation of the soft robotic arm.

C. Experiment of spatial posture

By inputting the rotation angles of the four servos, we can control the deflection and bending of the soft robotic arm. The vertical projection of the end is marked on a horizontal grid coordinate paper. Based on the projection mark, the x and y coordinates of the end are obtained for each posture. The vertical distance between the endpoint center and the base point O is measured as the z coordinate. Some spatial posture experiment results are shown in Fig. 6, with each spatial posture corresponding to the simulation results in Fig. 4. The simulation and experimental results are highly consistent, suggesting the rationality of the structural design and forward kinematics.

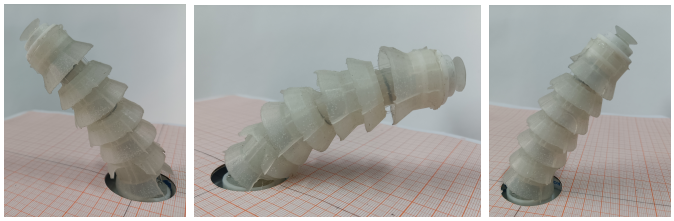

(a) (b) (c)

Fig. 6. Some experimental results of spatial posture.

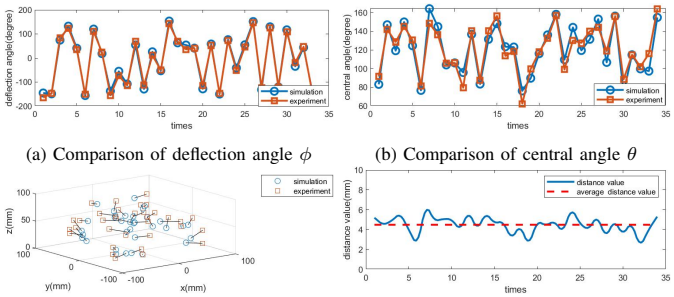

(a) Comparison of deflection angle ϕ (b) Comparison of central angle θ

(c) Comparison of endpoint position (d) Distance of endpoint position

Fig. 7. Comparison of spatial posture between simulation and experiment.

We conduct 34 spatial posture simulations and the corresponding experiments are carried out on the actual prototype. Fig. 7 (a), (b), and (c) show the comparison of deflection angle ϕ, central angle θ and endpoint position, respectively. And Fig. 7 (d) shows the distance of endpoint position between the simulation and experiment. It can be observed that the experimental data of the arm closely match the simulation data, further verifying the applicability of the model.

Kinematics is grounded on the assumption that the arm body bends with constant curvature. In addition, installation errors in actual prototype are caused, and there is motion friction during experiments. So there inevitably exist differences between the simulation and experimental results. Apart from minor data fluctuations, the error is in a reasonable range.

V. Verification of Inverse Kinematics

In this part, we perform circular trajectory planning to validate the correctness of inverse kinematic analysis. Firstly, determine the position and size of the theoretical circle based on the workspace, and select the circular trajectory points from the theoretical circle. Then, use inverse kinematics to obtain the corresponding inputs for each circular trajectory point. Finally, the simulation and experimental circular trajectories are obtained by using the above data, and compared with the theoretical circle to validate the rationality of inverse kinematics.

Within the workspace range shown in Fig. 5, we select some points to form an approximate circle, the spatial positions of the 12 points are shown as,

$$\begin{cases} \phi = t \cdot \pi/6 (t = 1, 2, \cdots, 12) \\ x = 85.75 \cos\phi, y = 85.75 \sin\phi, z = 49.6 \end{cases} \tag{16}$$

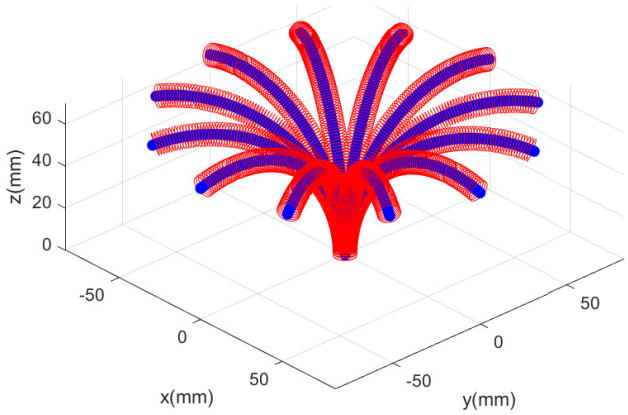

Fig. 8. Simulation postures corresponding to circular trajectory points.

As shown in Fig. 8, twelve points on a circle with the radius of 85.75mm are selected as the positions of the endpoints of the soft robotic arm. The 12 designated points distribute uniformly on a circle that is parallel to the xoy plane.

Through inverse kinematics calculation, the 12 sets of input angles of the servos can be obtained. The obtained data are input into the actual prototype to generate a series of spatial postures. Fig. 9 shows experimental postures corresponding to circular trajectory points.

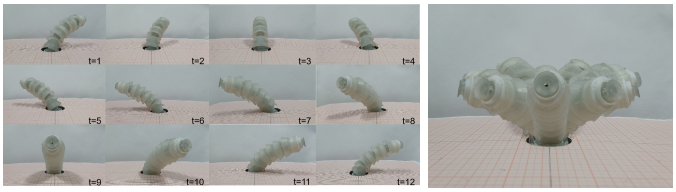

(a) 12 discrete postures (b) Composition diagram

Fig. 9. Experimental postures corresponding to circular trajectory points.

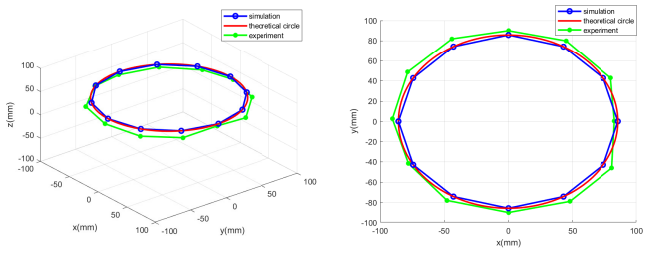

(a) Comparison of the results (b) Top view

Fig. 10. Comparison of theoretical circle with simulation and experimental results.

As shown in Fig. 10, the simulation and experimental polygonal trajectories are both approximate to theoretical circular trajectory. The result validates the applicability of inverse kinematics.

VI. Conclusion

In this paper, a rope-driven soft robotic arm is designed based on biological characteristics, and it can adapt to different working environments by adjusting its posture and can also realize two functions of wrapping and adsorbing objects, and the arm has a high degree of flexibility and adaptability. The kinematic analysis is carried out based on the constant curvature assumption. In addition, on the basis of discrete inputs, the experimental results and simulation results are highly consistent, which verifies the rationality of the structural design and the forward kinematic model. Finally, the applicability of inverse kinematics is proved through the experiment of circular trajectory. Further research on control algorithms and optimization of structural parameters will be conducted to improve the motion performance of the soft robotic arm.

References

[1] N. Gariya, P. Kumar, and R. Dobriyal, "A review on soft robotic technologies," AIP Conference Proceedings, vol. 2521, pp. 050004 (10 pp.), May 2023.

[2] D. Rus and M. T. Tolley, "Design, fabrication and control of soft robots," Nature, vol. 521, pp. 467-475, May 2015.

[3] H. Su, X. Hou, X. Zhang, et al, "Pneumatic soft robots: Challenges and benefits," Actuators, vol. 11, p. 92, March 2022.

[4] R. Wang, C. Zhang, W. Tan, and J. Yang, "Electroactive polymer-based soft actuator with integrated functions of multi-degree-of-freedom motion and perception," Soft Robotics, vol. 10, pp. 119-128, February 2023.

[5] Q. Wang, L. Yan, M. Li, H. Li, and B. Zhang, "Reliability Analysis of Continuum Robot Actuated by Shape Memory Alloy (SMA)," 2021 6th International Conference on Automation, Control and Robotics Engineering (CACRE), pp. 97-101, July 2021.

[6] B. Fang, F. Sun, L. Wu, et al, "Multimode grasping soft gripper achieved by layer jamming structure and tendon-driven mechanism," Soft Robotics, vol. 9, pp. 233-249, April 2022.

[7] A. Martin-Barrio, S. Terrile, M. Diaz-Carrasco, J. Cerro, and A. Barrientos, "Modelling the Soft Robot Kyma Based on Real-Time Finite Element Method," Computer Graphics Forum, vol. 39, pp. 289-302, May 2020.

[8] J. Bao, W. Chen, and J. Xu, "Kinematics modeling of a twisted and coiled polymer-based elastomer soft robot," IEEE Access, vol. 7, pp. 136792-136800, September 2019.

[9] X. Huang, J. Zou, and G. Gu, "Kinematic Modeling and Control of Variable Curvature Soft Continuum Robots," IEEE/ASME Transactions on Mechatronics, vol. 26, pp. 3175-3185, January 2021.

[10] G. Chen, X. Yang, Y. Xu, Y. Lu, and H. Hu, "Neural network-based motion modeling and control of water-actuated soft robotic fish," Smart Materials and Structures, vol. 32, pp. 015004 (11 pp.), December 2022.

[11] A. K. Schulz, J. N. Wu, S. Y. S. Ha, et al, "Suction feeding by elephants," Journal of the Royal Society Interface, vol. 18, June 2021.

[12] L. Wang, Z. Wang, B. Wang, et al, "Reversible adhesive bio-toe with hierarchical structure inspired by gecko," Biomimetics, vol. 8, January 2023.

[13] H. L. Liu, D. J. Kou, D. F. Yu, K. Y. Ge, and Y. M. Hu, "Kinematics and Dynamics Modeling and Analysis of Line-Driven Continuum Robot," 2020 5th International Conference on Automation, Control and Robotics Engineering (CACRE), pp. 97-100, September 2020.

[14] R. J. Webster III and B. A. Jones, "Design and kinematic modeling of constant curvature continuum robots: A review," International Journal of Robotics Research, vol. 29, pp. 1661-1683, June 2010.